applied sciences

MDPI

Article

A New Manipulator Calibration Method for the Identification of Kinematic and Compliance Errors Using Optimal Pose Selection

Phu-Nguyen Le [1] and Hee-Jun Kang [2,*]

[1] Department of Information Technology Specialization, FPT University, Hoa Lac High Tech Park, Hanoi 10000, Vietnam; nguyenlp9@fe.edu.vn
[2] Department of Electrical, Electronic and Computer Engineering, University of Ulsan, Ulsan 44610, Korea
* Correspondence: hjkang@ulsan.ac.kr

Abstract: In this study, a manipulator calibration algorithm is suggested to decrease the positional errors of an industrial robotic manipulator using a genetic algorithm to select optimal measurement poses. First, a genetic algorithm based on the observability index is used for the selection of optimal measurement poses. By employing the selected optimal poses, conventional kinematic calibration is used to identify the geometric errors of the robot. Finally, to further improve the positional accuracy of the robot, compliance errors are compensated by a radial basis function neural network based on effective torques. The proposed method provides a novel and effective way to select optimal measurement poses for the calibration process using a genetic algorithm and enhances the accuracy of the robot manipulators by constructing a relationship between the effective torque and the compliance errors using a radial basis function. The results of the experimental calibration and validation processes carried out on a YS100 robot show the effectiveness of the proposed method in comparison with the other calibration approaches.

Keywords: genetic algorithm; optimal measurement poses; robot accuracy; radial basis function; robot calibration

Citation: Le, P.-N.; Kang, H.-J. A New Manipulator Calibration Method for the Identification of Kinematic and Compliance Errors Using Optimal Pose Selection. *Appl. Sci.* **2022**, *12*, 5422. https://doi.org/10.3390/app12115422

Received: 4 April 2022
Accepted: 25 May 2022
Published: 27 May 2022

1. Introduction

Robot manipulators are extensively employed in industry. Although manipulators are extremely repeatable, their poor accuracy is well-known [1,2]. Research has shown that the primary potential sources of errors are geometric errors and non-geometric errors [3,4]. The sources of geometric errors are an erroneous production, assembly errors, and misalignment. Non-geometric errors occur because of elastic errors, alternating temperatures, gear transmission, and backlash [5].

The methods of geometric calibration have been commonly studied for decades. Denavit and Hartenberg proposed the D–H model [6], which is the most popular kinematic calibration process. Recently, Klug et al. used the D–H model to construct a full workflow for the automatic geometric model extraction of robotic total stations [7]. It has also been used by other researchers with modifications [8–10]. Researchers have also used other approaches for geometric calibration. A CPC model [11] was proposed by Zhang et al. to avoid model singularities owing to the implementation of direction vectors of the joint axes as link parameters. The POE method [12] was suggested by Park and Okamura to avoid the problem of singularity. It has been adopted in recent research [13,14]. Gupta proposed a zero-reference position method [15,16]. However, non-geometric defects were not considered in these calibration algorithms. Researchers have used different methods to examine joint compliance errors [17,18]. Nonetheless, these approaches do not take into account the effect of kinematic errors.

To investigate the influence of both kinematic and compliance errors, Zhou and Kang [19] suggested a method (SKCM) to simultaneously identify joint compliance and

kinematic parameters. However, the approach assumed that the joint compliance parameters were constant. In [9,20,21], calibration methods were proposed that considered both geometric and non-geometric errors. Meggiolaro et al. [22] suggested a procedure for approximating compliance errors where torque sensors were used through a polynomial equation of the joint and link parameters. These calibration methods have been successfully applied to industrial robotic manipulators, but the methods simply and randomly select the poses of the robot for the calibration process.

To perform robot calibration, the measurement is an important step. The collected measurement data are served as constraint equations on the parameters to be identified. However, the data acquisition for experimental robot calibration always contains noise. These inevitable errors degrade the calibration accuracy. To enhance the stability of the calibration algorithm with respect to measurement errors, Daney and Pagegay [23] increased the number of constraint equations. However, this approach took a lot of time and effort. Another approach is to improve the numerical quality of the measurements. To find an optimal set for robot configurations, numerous approaches have been used [24–26]. Recently, Jiang et al. suggested a calibration method for a serial robot that used a multiple identification space [24]. An optimization model with two observability indexes was introduced by Jia et al. [25]. A universal observability index was used in the work of Wang et al. [26]. These methods depend on the relevant observability index of the measurement configurations. A calibrated set that has a maximum observability index generates a better robustness of the calibration process. Nevertheless, the above methods only dealt with conventional kinematic calibration.

This work introduces a novel calibration method for improving the precision of robotic manipulators. An optimal robot configuration set was first selected by a genetic algorithm (GA) based on the observability index. GAs created by Holland and his colleagues [27] have been applied to numerous optimization problems. Due to the advantages of GAs [28]—such as parallel searching, stability for noise, and easy evasion from the local minima—configuration sets for optimal measurement poses were identified. Kinematic calibration was then used to determine the D-H constraints of the manipulator. Finally, using effective torques, a radial basis function (RBF) compensator was employed to compensate for the compliance errors.

Our method not only proposed the use of a GA for selecting the optimal poses to calibrate the robot, but also combined the optimal pose method and kinematic calibration method (KM). An RBF compensator was also used to compensate for the compliance errors using effective torques. This determined the optimal set of poses for calibration, identified the kinematic parameters, and compensated for the compliance errors. The benefits of the proposed algorithm were that it could find the highest observability index configuration set, it was easy to implement, it did not require torque sensors, and it improved the accuracy of the robot. The benefits of the proposed method were illustrated using a YS100 robot in comparison with the KM and SKCM [19].

The kinematic model of the YS100 robot is introduced in Section 2. In Section 3, the genetic algorithm is used to select the optimal measurement poses. Based on these optimal measurement poses, the RBF compensator that used effective torques is presented in Section 4. The experimental calibration results of the proposed method in comparison with other approaches is shown in Section 5. Finally, the conclusions are given in Section 6.

2. Kinematic Model of the YS100 Robot

In this work, a YS100 robot [19] was used to examine the proposed method. Figure 1 provides a sketch of the robot structure. The nominal parameters of it are shown in Table 1.

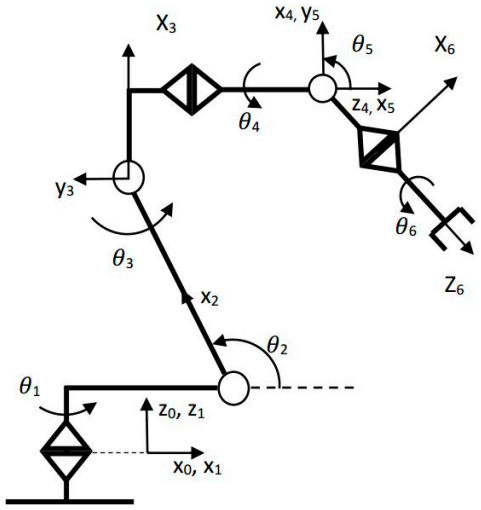

Figure 1. Sketch of a serial robot (YS100).

Table 1. Nominal D–H constraints of the YS100 robot.

i	α_{i-1} (deg)	a_{i-1} (m)	β_{i-1} (deg)	b_{i-1} (m)	d_i (deg)	θ_i (deg)
1	0	0	0	0	0.48	θ_1
2	90	0.32	-	-	0	θ_2
3	0	0.87	0	-	0	θ_3
4	90	0.2	-	-	1.03	θ_4
5	−90	0	-	-	0	θ_5
6	90	0	-	-	0.185	θ_6
T	-	0.2	-	0.05	0.5	-

The tool frame $\{T\}$ was related to the base frame $\{0\}$ by:

$$ {}^{0}_{T}\boldsymbol{T} = {}^{0}_{1}\boldsymbol{T}(\theta_1){}^{1}_{2}\boldsymbol{T}(\theta_2){}^{2}_{3}\boldsymbol{T}(\theta_3){}^{3}_{4}\boldsymbol{T}(\theta_4){}^{4}_{5}\boldsymbol{T}(\theta_5){}^{5}_{6}\boldsymbol{T}(\theta_6){}^{6}_{T}\boldsymbol{T} \tag{1} $$

The end-effector transformation was:

$$ ({}^{6}_{T})\boldsymbol{T} = \boldsymbol{T}r_X(a_6)\boldsymbol{T}r_Y(b_6)\boldsymbol{T}r_Z(d_7) \tag{2} $$

3. Selecting Optimal Measurement Poses by a Genetic Algorithm

Assuming m (the measurement pose) was used to calibrate the robotic manipulator, the dimension of the corresponding identification Jacobian matrix J was $3m \times n$ [29] (where only the position was considered) and n was the number of the identified parameters. Using the singular value decomposition method, the identification Jacobian matrix became:

$$ J = U\Sigma V \tag{3} $$

where U and V are orthonormal matrices. We assumed that $3m > n$, thus producing:

$$ \Sigma = \begin{pmatrix} \sigma_1 & 0 & \cdots & \cdots \\ \vdots & \vdots & \vdots & \vdots \\ 0 & 0 & \cdots & \sigma_n \\ 0 & 0 & \cdots & 0 \\ \vdots & \vdots & \vdots & \vdots \\ 0 & 0 & \cdots & 0 \end{pmatrix} \tag{4} $$

where Σ is a $3m \times n$ matrix and σ_i are singular values where $1 \leq i \leq n$.

Numerous observability indices were created using these singular values to quantify the quality of the pose selection. Menq et al. [30] suggested an observability index based on the sum of all singularities. The inverse condition number was used by Driels and Pathre [31]. Two observability indexes were suggested by Nahvi et al. [32].

In this work, an observability index based on the product of singular values was used [33]. It is known as the best observability index for minimizing the variance of parameters [34]. The observability index corresponded with the determinant of $J^T J$ and $\det(J^T J) = (\sigma_1 \cdots \sigma_n)^2$.

When the observability index was maximized, the errors of the parameters were best noticed.

$$O = \frac{(\sigma_1 \ldots \sigma_n)^{\frac{1}{n}}}{\sqrt{m}} \tag{5}$$

In [35], the observability (O) was approved to linearly correspond with the determinant of $J^T J$, invariant to scaling. This was the best observability index to minimize the variance of the parameters.

A GA is a well-known evolution method that is stimulated by the rule of natural selection. GAs mimic the selection process of nature. In the natural environment, individuals with the best fitness have a better chance of surviving. The genes of these individuals have a higher possibility of transferring to their successor. GAs include five phases:

- Initial population;
- Fitness function;
- Selection;
- Crossover;
- Mutation.

In this study, a GA was applied to find the best robot configuration set for the calibration process based on the observability index.

The process was as follows:

1. The pool of the configuration measurement, Ω, was initialized.
2. The population was generated, including an n individual. Each individual had an m configuration of measurements.
3. The fitness value of each individual based on the observability index, O, (Equation (5)) was then calculated.
4. Every individual was evaluated and ranked based on their fitness values.
5. When the terminating condition was reached, the process was stopped. The outputs were the set of the m configuration of measurements of the individual with the highest observability index, O.
6. The GA was used to produce the new population based on the observability index, O.
7. Steps 3–6 were repeated until the stopping criterion was satisfied.

In the steps of initializing and generating a new population by applying the genetic algorithm, each individual set had to be checked for duplicate configurations. If any robot configuration was replicated, its clone was eliminated and another configuration from the pool of configuration measurements (Ω) was added. The result of this step was that the robot configuration set had a maximum observability index, γ.

4. Identification of the Kinematic Parameters and Compliance Compensation Based on the Selected Optimal Measurement Poses

The end-effector position of the robot was calculated by Equation 6:

$$P_{real} = P_{kin} + \Delta P_{kin} + \Delta P_c + \Delta P_{extra} \tag{6}$$

where P_{kin} is the robot end-effector position that was obtained by the kinematic parameter and ΔP_{kin}, ΔP_c, and ΔP_{extra} are the position errors affected by the geometric errors, the joint compliance errors, and the unmodeled errors, respectively. The errors of the robot

end-effector mostly came from geometric errors and non-geometric errors. The geometric errors were well-calibrated by the conventional kinematic calibration. However, the non-geometric errors could not be neglected (in this work, the geometric errors and joint deflection errors were assumed to be dominant ΔP_{extra}). Therefore, Equation (6) could be rewritten:

$$\Delta P = \Delta P_{kin} + \Delta P_c = P_{real} - P_{kin} \tag{7}$$

Previous research [19] assumed that the joint could be modeled by a torsional spring with a constant compliance parameter. Therefore, the relationship of the position error caused by the joint compliance errors and the effective torques, τ, was linearized:

$$\Delta P_c = J_e \Delta \theta_c = J_e \tau C \tag{8}$$

where J_e, $\Delta\theta_c$, and C are the Jacobian matrix that relates the effective torque to the position errors affected by joint deflection [36], the joint deflection, and the vector of the joint compliance parameters, respectively.

To achieve a better positional accuracy, the RBF was used to construct compliance position errors caused by joint compliance errors based on the effective torque, τ.

Using the selected optimal poses with a maximum observability index, γ, from the previous section, the kinematic parameters of the robot could be identified using a kinematic calibration. The geometric errors, ΔP_{kin}, could be expressed as:

$$\Delta P_{kin} = J_{kin} \Delta \phi \tag{9}$$

where J_{kin} and $\Delta\phi$ are the kinematic Jacobian matrix and kinematic parameter error vector, respectively. The kinematic parameter error vector in Equation (9) could be identified using the iterative least squares method:

$$\Delta \phi = [(J^T J)^{-1} J^T] \Delta P \tag{10}$$

The residual positional error was calculated by:

$$\Delta P = P_m - P_{kin} \tag{11}$$

where P_m is the measured position vector.

After the kinematic calibration process, P_{kin} converged to the P_{kin}^c value. Therefore, the residual positional errors of the end-effector could be obtained by:

$$\Delta P_{res} = P_m - P_{kin}^c \tag{12}$$

In this work, the residual positional errors were assumed to occur from the compliance errors ($\Delta P_{res} = \Delta P_{mc}$). The joint compliance errors were also assumed to be the primary source of the compliance errors. Therefore, the positional errors due to joint deflections were considered to be equal to the residual positional errors, ΔP_{res}. To increase the precision of the robot, the non-linear relationship of the effective torque and the compliance errors were constructed by an RBF.

The RBF had six inputs and three outputs in this application. The inputs of the RBF were the effective torque of the joints; the outputs implied three elements of the position error vector. The total effective torques in the robot jth joint could be calculated by Equation (13):

$$\tau_i = \sum_{j=i}^{N+1} \tau_{i,j} = \sum_{j=i}^{N+1} {J_{\theta_{i,j}}}^T F_j \tag{13}$$

where $N = 6$ is the number of DOF of the robot and F_{N+1} is the gravity force due to the payload. Here, the gravity force accompanying the jth link was calculated by:

$$F_j = \begin{bmatrix} 0 & 0 & -M_j g \end{bmatrix} \tag{14}$$

where M_j and g are the mass of the link (jth) and the gravity coefficient, respectively.

The mass of the link vector was described as follows:

$$M = [196.7 \quad 79.25 \quad 170.27 \quad 10.58 \quad 22.33 \quad 2.0 \quad 110] \tag{15}$$

The Jacobian matrix in Equation (13) was calculated by:

$$J_{\theta_{i,j}} = z_i \times l_{i,j} \tag{16}$$

where z_i is the origin of the ith frame and $l_{i,j}$ is the 3×1 vector between the origin of the ith frame and was the mass center of the jth link.

The effective torques (Equation (13)) were the input of the RBF. This RBF was employed to construct the non-linear relationship, f_{RBF}, of the effective torques and the compliance errors:

$$\Delta P_c = f_{RBF}(\tau) \tag{17}$$

Figure 2 presents the form of the RBF. The output of the hidden node, i, could be obtained using Equation (18) [37]:

$$o_j = e^{-n^2} \tag{18}$$

where the transfer function, n, was obtained from Equation (19) [37]:

$$n = \|w_i - p\| b_i \tag{19}$$

where n, w_i, p, and b_i are the transfer function, weight vector, input vector, and bias, respectively.

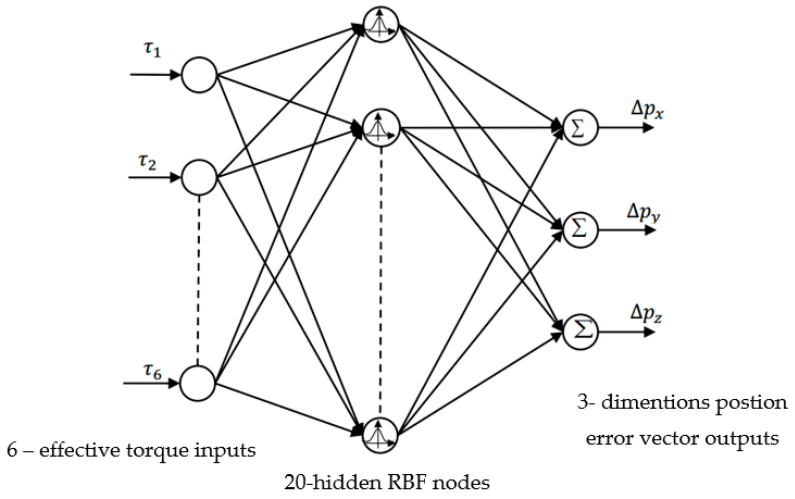

Figure 2. Kinematic structure of the RBF.

The output layer was a linear layer that had three linear nodes representing the positional error vector. The residual error of the robot end-effector after being compensated for by the RBF could be obtained by the following equation:

$$e = \Delta P_{res} - P_{nn} \tag{20}$$

The RBF was trained using the methods in previous works [37,38], using computed effective torques and residual errors. Generally, the proposed algorithm could be expressed by the flowchart in the Figure 3.

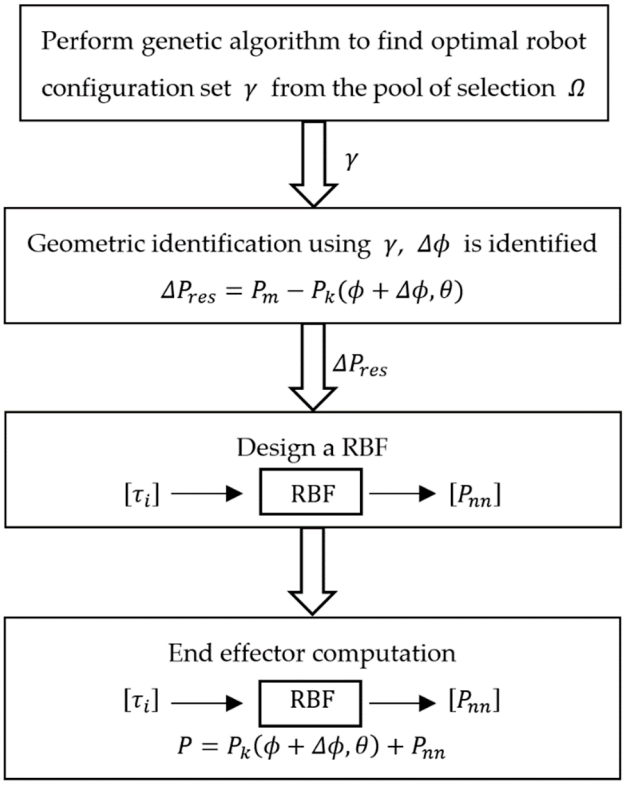

Figure 3. Flowchart of the proposed method.

5. Experiments and Results

To perform the calibration process, the experimental study was performed on a six DOF robot manipulator (YS100) carrying a heavy load. An API laser tracker (measurement accuracy of 0.01 mm/m, repeatability of ±0.006 mm/m) and an accompanying laser reflector attached to the end-effector of the robot were used for collecting the data. Figure 4 presents the experimental calibration setup.

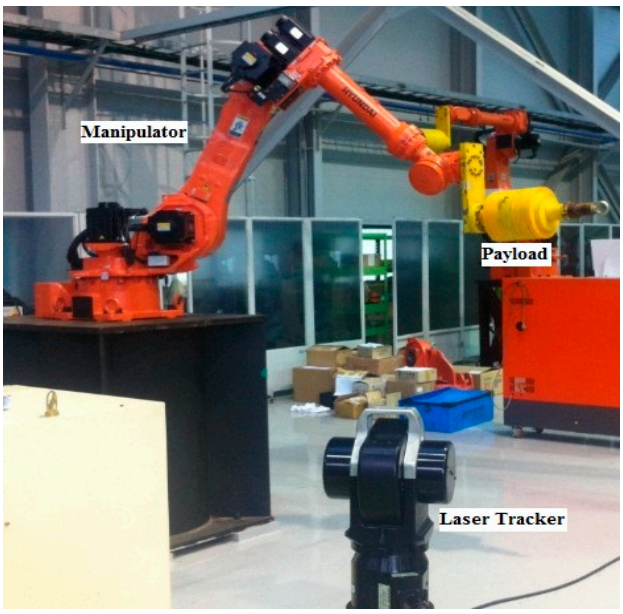

Figure 4. Experimental setup.

The proposed approach (GA-RBF-TCM) was examined on the YS100 robot in comparison with the kinematic calibration method (KM) and SKCM [19] in the experimental study.

The pool of robot configuration data contained 70 robotic configurations ($\Omega = 70$). These measurement settings were uniformly distributed around the accessible workspace. Due to barriers such as walls and neighboring manipulators in the workplace where the robot was positioned, the accessible workspace where the data measurements were taken was a sub-workspace of the full workspace in practice. Figure 5 shows the process of searching for 20 optimal poses by examining the genetic algorithm. In the next step, the set of 20 optimal poses (set Q_{OCal}) was used in the experimental calibration in contrast to other methods. The remaining 50 poses (Q_{OVal}) were used in the validation process.

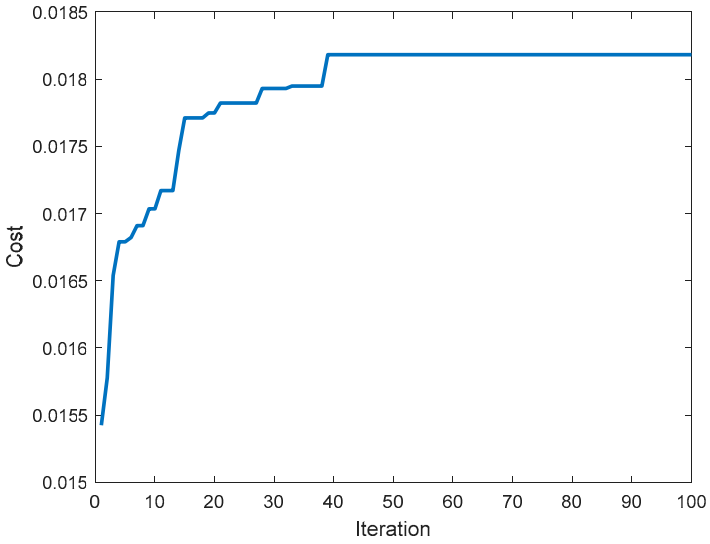

Figure 5. The process of searching for 20 optimal poses.

The initial values of the GA were population size $(n_{Pop} = 35)$, a crossover percentage equal to 85%, 35% mutation, and a mutation rate equal to 0.1. After 100 interactions, the observability index of the best set was $O = 0.0182$.

To confirm that the value of O was maximized, 1000 sets of robot configurations were randomly selected from the pool of robot configuration data. Figure 6 presents the result of the 1000 related values of the observability index related to the random set.

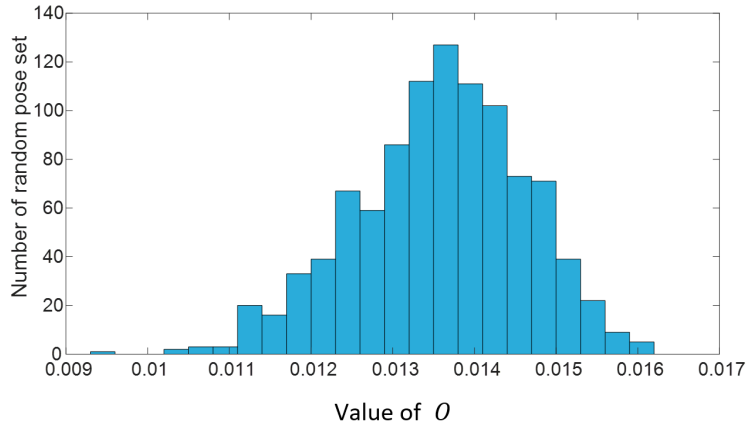

Figure 6. Result of the observability index related to 1000 random sets.

The maximum value of these observability indexes was 0.01613. The mean value was 0.01357. From the results of the selection process, the GA method showed its ability to determine the optimal poses with a maximum observability index value.

To confirm the ability of the proposed method for choosing optimal poses, an optimal set, Q_{OCal}, was used to calibrate the YS100 robot using the method in [35]. The remaining 50 poses (Q_{OVal}) were used in the validation process. In addition, a set of random poses, $Q_{randCal}$, including 20 poses from Ω, was taken to calibrate the robot using the kinematic calibration method (KM) and SKCM [19]. The non-selected 50 pose $Q_{randVal}$ was used to verify the calibration process. This random process was repeated 100 times. For each of the 100 random processes, the mean of the positional errors of the KM and SKCM methods was compared with the mean and maximum positional errors of the proposed method, both in the calibration and validation process.

Figure 7 shows the comparisons of the three methods in the calibration process. The mean of the positional error of the end-effector using the proposed method was 0.1603 mm.

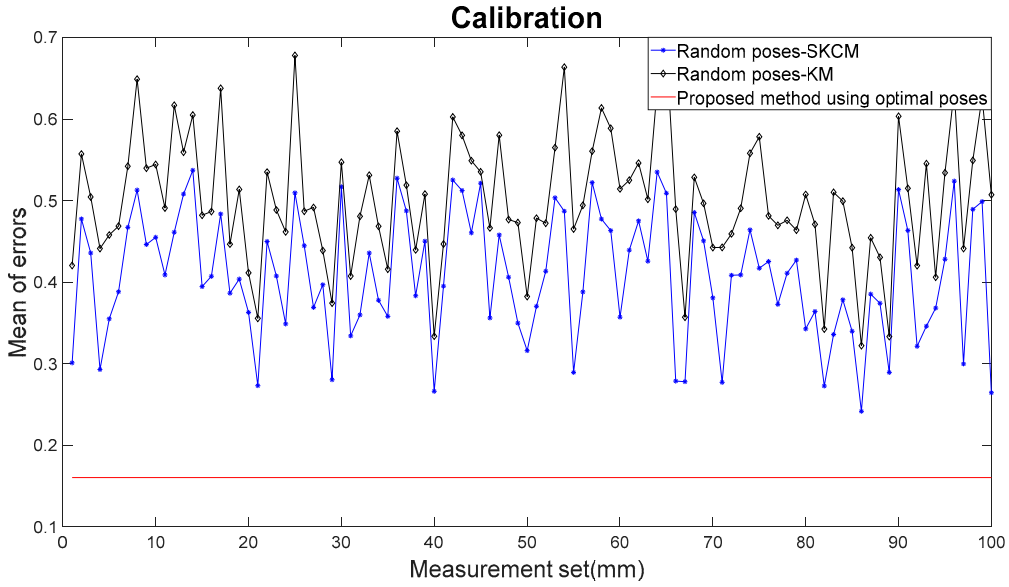

Figure 7. Result of the calibration process.

The maximum of the positional error of the end-effector was 0.3996 mm and the standard deviation of the positional error of the end-effector was 0.1011 mm. These results showed the effectiveness of the proposed method. It was easy to see from Figure 7 that the proposed technique outperformed the KM and SKCM methods. Using a 100 random set $Q_{randCal}$ for the calibration, the KM had the highest of the mean of errors at 0.68 mm; the lowest of the mean of errors was 0.32 mm and the average was about 0.5 mm. The SKCM had the highest of mean of errors at 0.54 mm; the lowest of the mean of errors was 0.24 mm and the average was about 0.41 mm. From these results, it was clear that the proposed method had a better effectiveness in contrast to the KM and SKCM methods. The results were confirmed again in the validation process.

Figure 8 shows the comparisons of the three methods in the validation process. The mean of the error using the proposed method was 0.2388 mm. The maximum of the error was 0.5930 mm and the standard deviation was 0.18 mm. These results were similar to the results of the calibration process. Using the 100 random set $Q_{randVal}$ for the calibration, the KM had the highest of the mean of errors at 2.18 mm; the lowest of the mean of errors was 0.75 mm and the average was about 1.06 mm. The SKCM had the highest of the mean of errors at 2.71 mm; the lowest of the mean of errors was 0.67 mm and the average was about 0.99 mm. From these results, it was clear that the proposed method had a better effectiveness in contrast to the KM and SKCM methods.

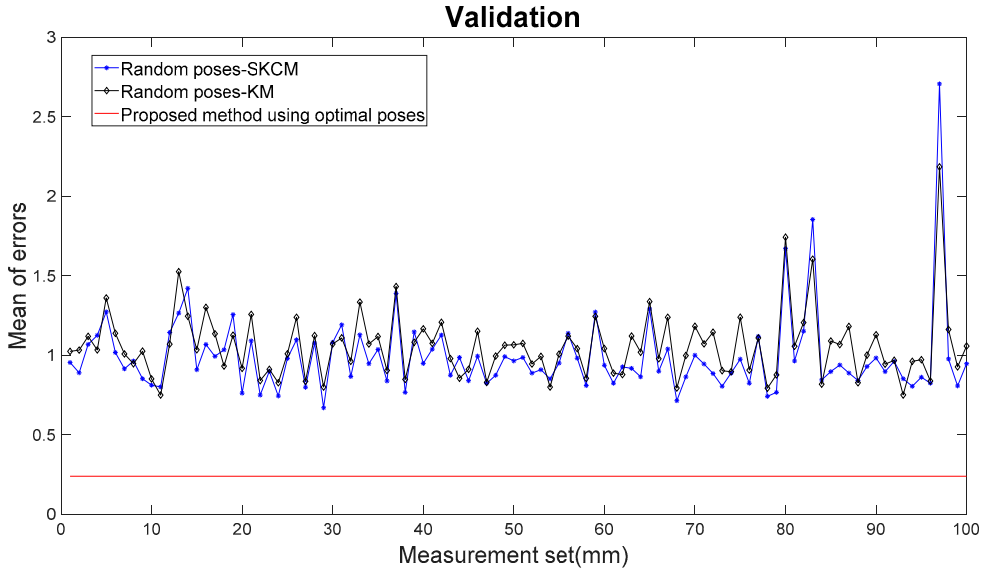

Figure 8. Result of the validation process.

6. Conclusions

This study proposed a new robot calibration approach to reduce positional errors using a genetic algorithm to select the optimal measurement poses. First, a genetic algorithm based on the observability index was used to select the optimal measurement poses. By employing the selected optimal poses, kinematic calibration was used to identify the geometric errors of the robot. Finally, to further improve the positional accuracy of the robot, the compliance errors were compensated for by a radial basis function based on the effective torques.

The proposed method provided an effective way to select the optimal measurement poses for the calibration process using a genetic algorithm. The suggested approach also constructed a relationship between the effective torque and the compliance errors using an RBF. The benefits of the proposed approach are that it is simple to implement, it does not require torque sensors, and it has a high capacity to increase the accuracy of the robot. The results of the experimental calibration and validation processes carried out on a YS100 robot showed the improved positional accuracy of the robot manipulator using the proposed algorithm over the other robotic manipulator calibration approaches.

Author Contributions: Conceptualization, P.-N.L.; Supervision, H.-J.K.; Writing—original draft, P.-N.L.; Writing—review & editing, H.-J.K. All authors have read and agreed to the published version of the manuscript.

Funding: This research was funded by the Ministry of Education (NRF-2019R1D1A3A03103528) in South Korea.

Institutional Review Board Statement: Not applicable.

Informed Consent Statement: Not applicable.

Conflicts of Interest: The authors declare no conflict of interest.

References

1. Kim, S.H.; Nam, E.; Ha, T.I.; Hwang, S.-H.; Lee, J.H.; Park, S.-H.; Min, B.-K. Robotic machining: A review of recent progress. *Int. J. Precis. Eng. Manuf.* **2019**, *20*, 1629–1642. [CrossRef]
2. Shu, T.; Gharaaty, S.; Xie, W.; Joubair, A.; Bonev, I.A. Dynamic path tracking of industrial robots with high accuracy using photogrammetry sensor. *IEEE/ASME Trans. Mechatron.* **2018**, *23*, 1159–1170. [CrossRef]
3. Shi, X.J.; Zhang, F.M.; Qu, X.; Liu, B.; Wang, J. Position and attitude measurement and online errors compensation for KUKA industrial robots. *Chin. J. Mech. Eng.* **2017**, *53*, 1–7. [CrossRef]

4. Zeng, Y.; Tian, W.; Li, D.; He, X.; Liao, W. An error-similarity-based robot positional accuracy improvement method for a robotic drilling and riveting system. *Int. J. Adv. Manuf. Technol.* **2017**, *88*, 2745–2755. [CrossRef]
5. Nguyen, H.X.; Cao, H.Q.; Nguyen, T.T.; Tran, T.N.-C.; Tran, H.N.; Jeon, J.W. Improving Robot Precision Positioning Using a Neural Network Based on Levenberg Marquardt—APSO Algorithm. *IEEE Access* **2021**, *9*, 75415–75425. [CrossRef]
6. Denavit, J.; Hartenberg, R.S.; Mooring, B.W.; Tang, G.R.; Whitney, D.E.; Lozinski, C.A. A kinematic notation for low pair mechanisms based on matrices. *J. Appl. Mech.* **1955**, *77*, 215–221. [CrossRef]
7. Klug, C.; Schmalstieg, D.; Gloor, T.; Arth, C. A complete workflow for automatic forward kinematics model extraction of robotic total stations using the Denavit-Hartenberg convention. *J. Intell. Robot. Syst.* **2019**, *95*, 311–329. [CrossRef]
8. Chen, K.; Zhan, K.; Yang, X.; Zhang, D. Accuracy Improvement Method of a 3D Laser Scanner Based on the DH Model. *Shock Vib.* **2021**, *2021*, 9965904.
9. Wang, Z.; Chen, Z.; Wang, Y.; Mao, C.; Hang, Q. A robot calibration method based on joint angle division and an artificial neural network. *Math. Probl. Eng.* **2019**, *2019*, 9293484. [CrossRef]
10. Zu, H.; Chen, X.; Chen, Z.; Wang, Z.; Zhang, X. Positioning accuracy improvement method of industrial robot based on laser tracking measurement. *Meas. Sens.* **2021**, *18*, 100235. [CrossRef]
11. Zhuang, H.; Wang, L.K.; Roth, Z.S. Error-model-based robot calibration using a modified CPC model. *Robot. Comput. Integr. Manuf.* **1993**, *10*, 287–299. [CrossRef]
12. Okamura, K.; Park, F.C. Kinematic calibration using the product of exponentials formula. *Robotica* **1996**, *14*, 415–421. [CrossRef]
13. Chen, G.; Kong, L.; Li, Q.; Wang, H.; Lin, Z. Complete, minimal and continuous error models for the kinematic calibration of parallel manipulators based on POE formula. *Mech. Mach. Theory* **2018**, *121*, 844–856. [CrossRef]
14. Wang, H.; Lu, X.; Sheng, C.; Zhang, Z.; Cui, W.; Li, Y. General frame for arbitrary 3R subproblems based on the POE model. *Rob. Auton. Syst.* **2018**, *105*, 138–145. [CrossRef]
15. Gupta, K.C. Kinematic analysis of manipulators using the zero reference position description. *Int. J. Rob. Res.* **1986**, *5*, 5–13. [CrossRef]
16. Cheng, L.-P.; Kazerounian, K. Study and enumeration of singular configurations for the kinematic model of human arm. In Proceedings of the IEEE 26th Annual Northeast Bioengineering Conference (Cat. No. 00CH37114), Storrs, CT, USA, 9 April 2000; pp. 3–4.
17. Bai, Y.; Wang, D. Using Shallow Neural Network Fitting Technique to Improve Calibration Accuracy of Modeless Robots. In Proceedings of the IFIP International Conference on Artificial Intelligence Applications and Innovations, Hersonissos, Greece, 24–26 May 2019; pp. 623–631.
18. Bai, Y.; Wang, D. On The Comparison of Fuzzy Interpolations and Neural Network Fitting Functions in Modeless Robot Calibrations. In Proceedings of the 2019 IEEE International Conference on Fuzzy Systems (FUZZ-IEEE), New Orleans, LA, USA, 23–26 June 2019; pp. 1–6.
19. Zhou, J.; Nguyen, H.-N.; Kang, H.-J. Simultaneous identification of joint compliance and kinematic parameters of industrial robots. *Int. J. Precis. Eng. Manuf.* **2014**, *15*, 2257–2264. [CrossRef]
20. Cao, C.-T.; Do, V.-P.; Lee, B.-R. A novel indirect calibration approach for robot positioning error compensation based on neural network and hand-eye vision. *Appl. Sci.* **2019**, *9*, 1940. [CrossRef]
21. Le, P.-N.; Kang, H.-J. A Robotic Calibration Method Using a Model-Based Identification Technique and an Invasive Weed Optimization Neural Network Compensator. *Appl. Sci.* **2020**, *10*, 7320. [CrossRef]
22. Meggiolaro, M.A.; Dubowsky, S.; Mavroidis, C. Geometric and elastic error calibration of a high accuracy patient positioning system. *Mech. Mach. Theory* **2005**, *40*, 415–427. [CrossRef]
23. Daney, D.; Papegay, Y.; Madeline, B. Choosing measurement poses for robot calibration with the local convergence method and Tabu search. *Int. J. Rob. Res.* **2005**, *24*, 501–518. [CrossRef]
24. Jiang, Z.; Huang, M.; Tang, X.; Song, B.; Guo, Y. Observability index optimization of robot calibration based on multiple identification spaces. *Auton. Robots* **2020**, *44*, 1029–1046. [CrossRef]
25. Jia, Q.; Wang, S.; Chen, G.; Wang, L.; Sun, H. A novel optimal design of measurement configurations in robot calibration. *Math. Probl. Eng.* **2018**, *2018*, 4689710. [CrossRef]
26. Wang, W.; Song, H.; Yan, Z.; Sun, L.; Du, Z. A universal index and an improved PSO algorithm for optimal pose selection in kinematic calibration of a novel surgical robot. *Robot. Comput. Integr. Manuf.* **2018**, *50*, 90–101. [CrossRef]
27. Holland, J.H. Genetic algorithms and the optimal allocation of trials. *SIAM J. Comput.* **1973**, *2*, 88–105. [CrossRef]
28. Srinivas, M.; Patnaik, L.M. Genetic algorithms: A survey. *Computer* **1994**, *27*, 17–26. [CrossRef]
29. Khalil, W.; Gautier, M.; Enguehard, C. Identifiable parameters and optimum configurations for robots calibration. *Robotica* **1991**, *9*, 63–70. [CrossRef]
30. Menq, C.-H.; Borm, J.-H.; Lai, J.Z. Identification and observability measure of a basis set of error parameters in robot calibration. *J. Mech. Transm. Autom. Des.* **1989**, *111*, 513–518. [CrossRef]
31. Driels, M.R.; Pathre, U.S. Significance of observation strategy on the design of robot calibration experiments. *J. Robot. Syst.* **1990**, *7*, 197–223. [CrossRef]
32. Nahvi, A.; Hollerbach, J.M.; Hayward, V. Calibration of a parallel robot using multiple kinematic closed loops. In Proceedings of the 1994 IEEE International Conference on Robotics and Automation, San Diego, CA, USA, 8–13 May 1994; pp. 407–412.

33. Borm, J.-H.; Menq, C.-H. Experimental study of observability of parameter errors in robot calibration. In Proceedings of the 1989 IEEE International Conference on Robotics and Automation, Scottsdale, AZ, USA, 14–19 May 1989; pp. 587–588.
34. Sun, Y.; Hollerbach, J.M. Observability index selection for robot calibration. In Proceedings of the 2008 IEEE International Conference on Robotics and Automation, Pasadena, CA, USA, 19–23 May 2008; pp. 831–836.
35. Zhou, J.; Nguyen, H.-N.; Kang, H.-J. Selecting optimal measurement poses for kinematic calibration of industrial robots. *Adv. Mech. Eng.* **2014**, *6*, 291389. [CrossRef]
36. Nakamura, Y.; Ghodoussi, M. Dynamics computation of closed-link robot mechanisms with nonredundant and redundant actuators. *Int. Conf. Robot. Autom.* **1989**, *5*, 294–302. [CrossRef]
37. Le, P.-N.; Kang, H.-J. A New Hybrid Calibration Method for Robot Manipulators by Combining Model–Based Identification Technique and a Radial Basis Function–Based Error Compensation. In Proceedings of the International Conference on Intelligent Computing, Nanchang, China, 3–6 August 2019; pp. 20–31.
38. Le, P.-N.; Kang, H.-J. A New Robotic Manipulator Calibration Method of Identification Kinematic and Compliance Errors. In Proceedings of the International Conference on Intelligent Computing, Bari, Italy, 2–5 October 2020; pp. 16–27.